scientific reports

Check for updates

OPEN

Gas discrimination by simultaneous sound velocity and attenuation measurements using uncoated capacitive micromachined ultrasonic transducers

Luis Iglesias Hernandez[1], Priyadarshini Shanmugam[2], Jean-François Michaud[2], Daniel Alquier[2], Dominique Certon[2] & Isabelle Dufour[1]✉

Chemically functionalized or coated sensors are by far the most employed solution in gas sensing. However, their poor long term stability represents a concern in applications dealing with hazardous gases. Uncoated sensors are durable but their selectivity is poor or non-existent. In this study, multi-parametric discrimination is used as an alternative to selectivity for uncoated capacitive micromachined ultrasonic transducers (CMUTs). This paper shows how measuring simultaneously the attenuation coefficient and the time of flight under different nitrogen mixtures allows to identify hydrogen, carbon dioxide and methane from each other and determine their concentration along with identification of temperature and humidity drifts. Theoretical comparison and specific signal processing to deal with the issue of multiple reflections are also presented. Some potential applications are monitoring of refueling stations, vehicles and nuclear waste storage facilities.

Nowadays, most gas sensors present a chemical component such as a functionalized coating specifically engineered to target a particular analyte[1,2]. However, it is well known that such chemical coating presents long term stability issues[3]. This results in the need for recalibrating the sensor, typically every couple of months. For applications dealing with hazardous gases such as hydrogen, H_2, or methane, CH_4, this becomes dangerous for the operators. Alternatively, it is possible to compensate this drift digitally, for instance, with artificial intelligence[4] or sophisticated models[5]. Nevertheless, this naturally increases both the manufacturing and the development cost. For this reason and despite their typically lower selectivity and worse limits of detection (LOD)[2], the development of uncoated gas sensors has increased in popularity over the past decade. Indeed, some parameters such as the resonant frequency of a cantilever[6], the gas sound velocity[7] and the acoustic attenuation coefficient[8,9] depend on the gas physical properties. This allowed the development of gas density sensors[10] and in some cases these principles can be exploited to measure a binary gas mixture concentration[11,12]. Some of these sensors consist of capacitive micromachined ultrasonic transducers (CMUTs)[13]. Typical LODs associated to uncoated sensors go from 3% down to 100 ppm and they are usually considered as non selective. However, in some specific cases, uncoated sensors can show performances close to coated sensors such as a LOD of a few ppm[14] and even selectivities higher than 10[15]. In order to overcome the problem of selectivity, an alternative consists in discrimination by measuring multiple physical properties of a gas mixture such as mass density and viscosity[16]. In this paper, we propose to measure simultaneously two other gas properties; the acoustic attenuation coefficient, α, for frequencies ranging from 1 to 4.5 MHz, and the time of flight, τ, which is the time taken by an acoustic ultrasonic wave to travel from an emitter to a receiver passing through the gas to be characterized. In such a setup, α can be defined as:

$$\alpha = \frac{1}{d} ln \frac{P_e}{P_r}, \tag{1}$$

where d is the distance between the emitter and the receiver and P_e and P_r are the amplitudes of the acoustic wave at the emission and the reception ends, respectively. This work is the continuation of previous work showing the

[1]Laboratoire IMS UMR-CNRS 5218, University of Bordeaux, 351 cours de la libération, 33405 Talence Cedex, France. [2]GREMAN, UMR-CNRS 7347, University of Tours, 16 rue Pierre et Marie Curie, BP 7155, 37071 Tours Cedex 2, France. ✉email: isabelle.dufour@ims-bordeaux.fr

possibility to use CMUTs to determine the concentration of a binary gas mixture by measuring either τ[17,18] or α[15] separately and in which the best selectivity obtained was slightly over 10. Although this value is high enough for some applications, it can be considered very low for others. For this reason, a setup capable of measuring both properties, time of flight and attenuation coefficient, is presented in this study. The choice of using CMUTs comes from several advantages over other ultrasonic transducers such as piezoelectric based ultrasonic transducers. These are easier to integrate and present a wider bandwidth, which allows to perform gas measurements over a larger part of the attenuation spectrum[19]. "Results" section shows characterization of the sensor regarding the influence of the temperature and humidity on the sensor and its sensitivity for three mixtures of nitrogen, N_2, with either hydrogen, H_2, carbon dioxide, CO_2, or methane, CH_4. The choice of N_2 as the main gas is done in order to simplify the modeling and due to its similarity to air in terms of acoustical properties. In "Discussion" section, based on the results, the advantages of measuring simultaneously τ and α, are discussed. Finally, in "Methods" section, details are given about the setup such as the microfabrication of the CMUTs and the signal processing employed for a robust measurement, even in case of spurious reflections and electrical coupling between the emitter and the receiver.

Results

Details on how both the time of flight, τ, and the shift in attenuation with respect to pure nitrogen at 20 °C, $\Delta\alpha$, are measured can be found in "Methods" section along with detailed information about the setup and the CMUT arrays.

Temperature and humidity characterization. This section seeks to estimate the sensor cross-sensitivity to the temperature, T, between 20 and 50 °C of both the measurement of τ, S_τ^T, and of $\Delta\alpha$, S_α^T as well as the cross-sensitivities to the relative humidity, RH, noted S_τ^{RH} and S_α^{RH}. In order to achieve this, both τ and $\Delta\alpha$ where measured at different temperatures under pure dry N_2 in that temperature range. The resulting characteristics are shown in Fig. 1a,b. Similarly, both quantities, τ and $\Delta\alpha$, were measured at 20 °C with RH going from 0% to about 50% (Fig. 1c,d).

In the case of the measurement of τ, the theoretical value can be estimated for an ideal gas by exploiting Newton–Laplace formula for the sound velocity, v, of an ideal gas[7]:

$$v = \sqrt{\frac{\gamma P}{\rho}} = \sqrt{\frac{\gamma RT}{M}}, \tag{2}$$

where P is the atmospheric pressure, ρ the gas mass density, γ the heat capacities ratio (considered constant in this range of temperature) and M the molar mass of the gas. Differentiating Eq. (2) results in:

$$\frac{\Delta v}{v} = \frac{1}{2}\frac{\Delta T}{T}, \tag{3}$$

where Δv and ΔT are small variations of v and T, respectively. Since $v = d/\tau$,

$$\frac{\Delta v}{v} = -\frac{\Delta \tau}{\tau}, \tag{4}$$

where $\Delta\tau$ represents small variations of τ. Finally, S_τ^T is given by:

$$S_\tau^T = \frac{\Delta \tau}{\Delta T} = -\frac{1}{2}\frac{\tau}{T} \tag{5}$$

For pure nitrogen at 20 °C, $\tau = 21.35\,\mu$s (distance $d \approx 7.5$ mm), the theoretical value is $S_\tau^T = -36$ ns/K against the experimental value of -31 ns/K. The difference might come from the relatively large temperature variation range or the fact that the sensor and the thermocouple used to measure the temperature are a few centimeters apart inside the oven. However, as it will be shown later, this difference is sufficiently small for the purpose of this article.

In the case of the humidity, one can express the variations of τ with respect to the molar fraction of vapor water x_w in N_2[17],

$$\frac{\Delta \tau}{\Delta x_w} = \frac{\tau}{2}\left[\frac{\rho^w}{\rho^{N2}} + \frac{c_v^w}{c_v^{N2}} - \frac{c_p^w}{c_p^{N2}} - 1\right], \tag{6}$$

where $\rho^w = 0.739$ kg/m^3[20], $c_p^w = 1.97$ kJ/K/kg[20], $c_v^w = 1.50$ kJ/K/kg[20] are the mass density, the isobaric heat capacity and the isochoric heat capacity of water vapor, respectively and $\rho^{N2} = 1.16$ kg/m^3[20], $c_p^{N2} = 1.04$ kJ/K/kg[20], $c_v^{N2} = 0.743$ kJ/K/kg[20] the same properties for N_2. Since RH is the mass of water in the gas with respect to the maximum amount of water that can be diluted in N_2, it is given by[20]:

$$RH = \frac{\rho^w x_w}{\rho_{max}}, \tag{7}$$

with

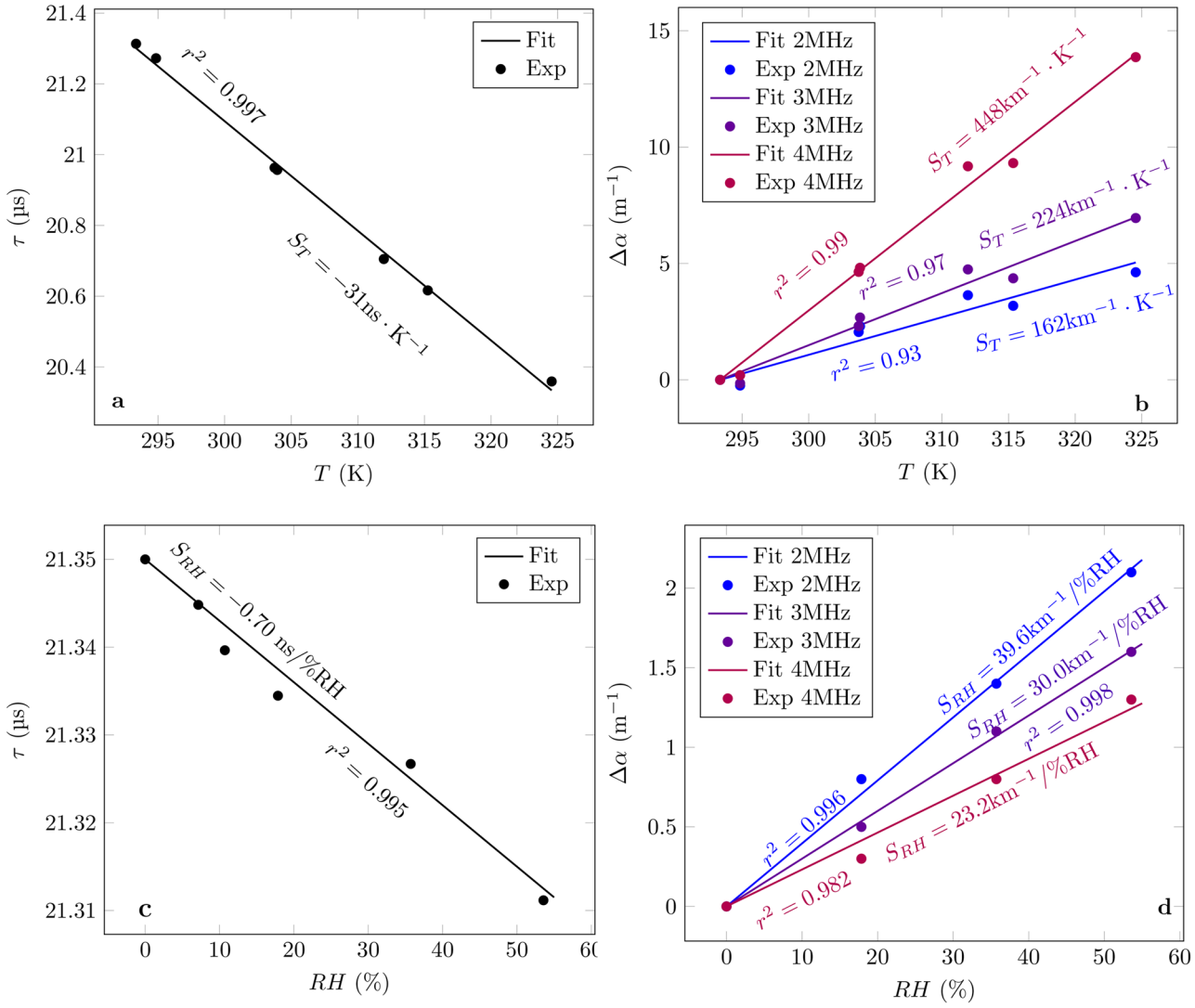

Figure 1. Sensor response to temperature under pure N_2: (**a**) time of flight and (**b**) attenuation shift. Sensor response to humidity under pure N_2: (**c**) time of flight and (**d**) attenuation shift.

$$\rho_{max} = \frac{P_s M_w}{RT}, \tag{8}$$

where $P_s = 2310$ Pa[20] is the saturated water vapor pressure at 20 °C and $M_w = 18.02$ g/mol[20] the molar mass of water. Therefore the sensitivity of τ to RH is:

$$S_\tau^{RH} = \frac{\Delta\tau}{\Delta RH} = \frac{\rho_{max}}{\rho^w}\frac{\tau}{2}\left[\frac{\rho^w}{\rho^{N2}} + \frac{c_v^w}{c_v^{N2}} - \frac{c_p^w}{c_p^{N2}}\cdot - 1\right], \tag{9}$$

Once again the measured value of − 0.70 ns/%RH is consistent with the theoretical one of − 0.69 ns/%RH.

In the case of $\Delta\alpha$, due to the complexity of its analytical expression and its dependence on an important number of gas properties, the temperature and humidity influence on the attenuation in this study is purely experimental. From Fig. 1, it can be concluded that, in the range between 2 and 4 MHz, the sensor's temperature cross-sensitivity increases with the frequency whereas the one of humidity follows the opposite behaviour. Their values will be exploited in the following section.

Gas characterization. The temperature and humidity influence on the sensor being known, this section aims to characterize the sensor response to different gas mixtures. For that, the sensor was exposed to sequences where pure N_2 is alternated with binary mixtures of N_2 with either H_2, CO_2 or CH_4 at different molar concentrations, x of the targeted gas. An example of the measurements at 4 MHz is shown in Fig. 2 for both, (a) the shift in time of flight with respect to N_2, $\Delta\tau$, and (b) $\Delta\alpha$. From these measurements one can extract the sensitivities through calibration curves, both of $\Delta\tau$ (c) and $\Delta\alpha$ (d) to the targeted gas (H_2, CO_2 or CH_4), S_τ and S_α, respectively. Although a complete study on the sensor drift (particularly degradation of the mechanical properties of

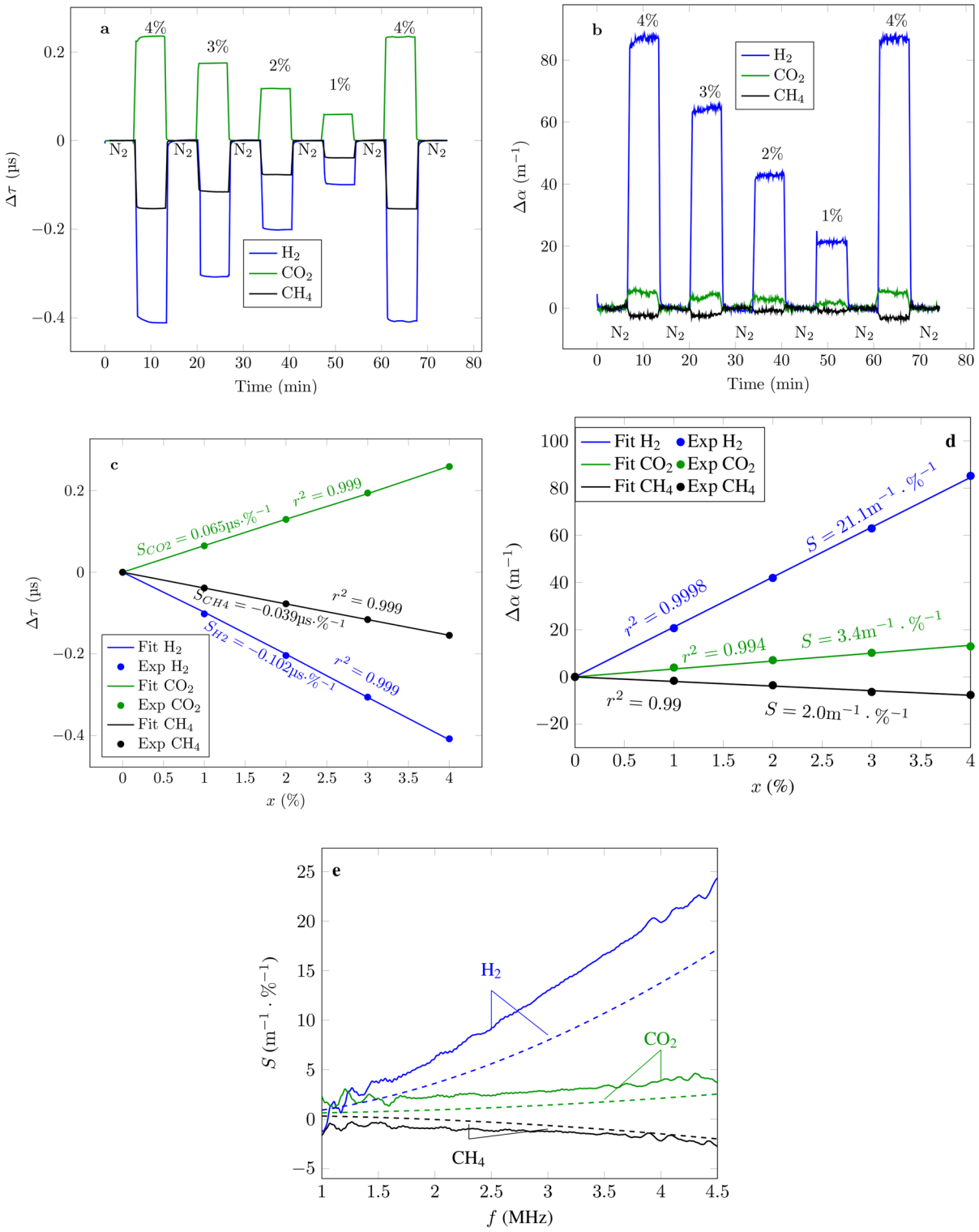

Figure 2. Sensor response to binary mixtures of N_2 with either H_2, CO_2 or CH_4. (**a**) Shift in time of flight when alternating the mixture at different concentrations with pure N_2. (**b**) Attenuation shift at 4 MHz when alternating the mixture at different concentrations with pure N_2. (**c**) Calibration curves from (**a**). (**d**) Calibration curves from (**b**). (**e**) Experimental (solid lines) and theoretical (dashed lines) values of the sensor sensitivity in attenuation shift as a function of the excitation frequency for the three binary gas mixtures.

Property	N_2	H_2	CO_2	CH_4
ρ (kg/m^3)	1.16[20]	0.0827[20]	1.82[20]	0.68[20]
η (μPa.s)	17.6[20]	8.8[20]	14.7[20]	11.0[20]
η_v (μPa.s)	12.8[26]	265[26]	5.4[27]	14.5[26]
K (W/K/m)	0.024[20]	0.168[20]	0.015[20]	0.030[20]
c_p (kJ/K/kg)	1.04[20]	14.3[20]	0.844[20]	2.22[20]
c_v (kJ/K/kg)	0.743[20]	10.2[20]	0.655[20]	1.70[20]
γ (×1)	1.4[20]	1.4[20]	1.3[20]	1.3[20]
v (m/s)	349[20]	1306[20]	267[20]	445[20]
f_{vr}	0.01 Hz[28]	13 MHz[29]	30 kHz[8]	150 kHz[8]
A (×1)	6×10^{-4}[28]	0.56[29]	0.24[8]	6.6×10^{-2}[8]
M (g/mol)	28[20]	2[20]	44[20]	16[20]
δ (cm^2/s)	NA	0.77[30]	0.15[30]	0.22[30]
a (×1)	NA	0.26[31]	0.065[32]	0.070[33]

Table 1. Physical properties of gases.

the membrane) is out of the scope of this work, it should be noted that, at constant temperature with dry gases, no detectable drift was observed for several hours of experiment. This emphasizes one of the advantages of uncoated sensors with respect to functionalized sensors.

Since S_α depends on the excitation frequency, it was measured for the whole frequency range of 1 MHz up to 4.5 MHz (e) which is limited by the charge amplifier at the lower end and by the strong attenuation above 4.5 MHz. Such frequency range is convenient to prevent typical vibration sources to interfere with the measurements[21] although it might not be adapted for applications where other ultrasonic sources on the same frequency range as the measurements are present. Similarly to the derivation of the expression of the humidity cross-sensitivity, the expression of S_τ can be obtained[17]:

$$S_\tau = \frac{\Delta\tau}{x} = \frac{\tau}{2}\left[\frac{\rho^G}{\rho^{N2}} + \frac{c_v^G}{c_v^{N2}} - \frac{c_p^G}{c_p^{N2}} - 1\right], \tag{10}$$

where c_p^G and c_v^G are the isobaric and isochoric heat capacities per unit mass of the targeted pure gas, respectively, and c_p^{N2} and c_v^{N2} the ones of pure N_2. To derive an exact expression of S_α would be unnecessarily complex. Therefore, in this study, a simple model is used from the expression of the attenuation of a pure gas α_p[22]:

$$\alpha_p = \frac{2\pi^2 f^2}{\rho v^3}\left(\frac{4}{3}\eta + \eta_v + \frac{\gamma-1}{c_p}K\right) + \alpha_{vr}, \tag{11}$$

where η is the viscosity of the gas, η_v its volume viscosity, K its thermal conductivity, c_p its isobaric heat capacity per unit mass and α_{vr} the vibrational relaxation attenuation contribution modeled as[23]:

$$\alpha_{vr} = \frac{Af}{v}\frac{f/f_{vr}}{1+f^2/f_{vr}^2}, \tag{12}$$

where A is a constant depending on the strength of the relaxation process and f_{vr} the frequency corresponding to the maximum of the normalized attenuation coefficient $\alpha v/f$. When dealing with a binary gas mixture, an additional contribution of the diffusion process α_δ is needed, especially for molecules with very different molar masses M such as H_2 and N_2[24]:

$$\alpha_\delta = \frac{2\pi^2 f^2}{\rho v^3} x(1-x)\gamma\delta\left(\frac{\Delta M}{M} + \frac{\gamma-1}{\gamma}a\right)^2, \tag{13}$$

where a is the thermal diffusion factor of the mixture, δ its diffusion coefficient and ΔM is the difference in molar masses between both constituents of the mixture. The shift in attenuation with respect to N_2 is then approximated to:

$$\Delta\alpha = [x\alpha_G + (1-x)\alpha_{N2} + \alpha_\delta] - \alpha_{N2}, \tag{14}$$

where α_{N2} and α_G are the attenuation coefficients in the pure state of N_2 and the targeted gas respectively, as given by Eq. (11). Finally, S_α is simply $\Delta\alpha(x = 1\%)$.

All the necessary constants to compute both S_τ and S_α for the three mixtures studied in this article are given in Table 1. From them the theoretical values of S_τ for the mixtures, N_2–H_2, N_2–CO_2 and N_2–CH_4, are − 100 ns/%, 72 ns/% and − 35 ns/%, respectively. The measurements (Fig. 2c) are consistent with the theory. Additionally, in Fig. 2e, the theoretical values of S_α are displayed in dashed lines along with the measured results. Once again the results are consistent with the theory in terms of sign and the overall form of the variation. In the case of H_2,

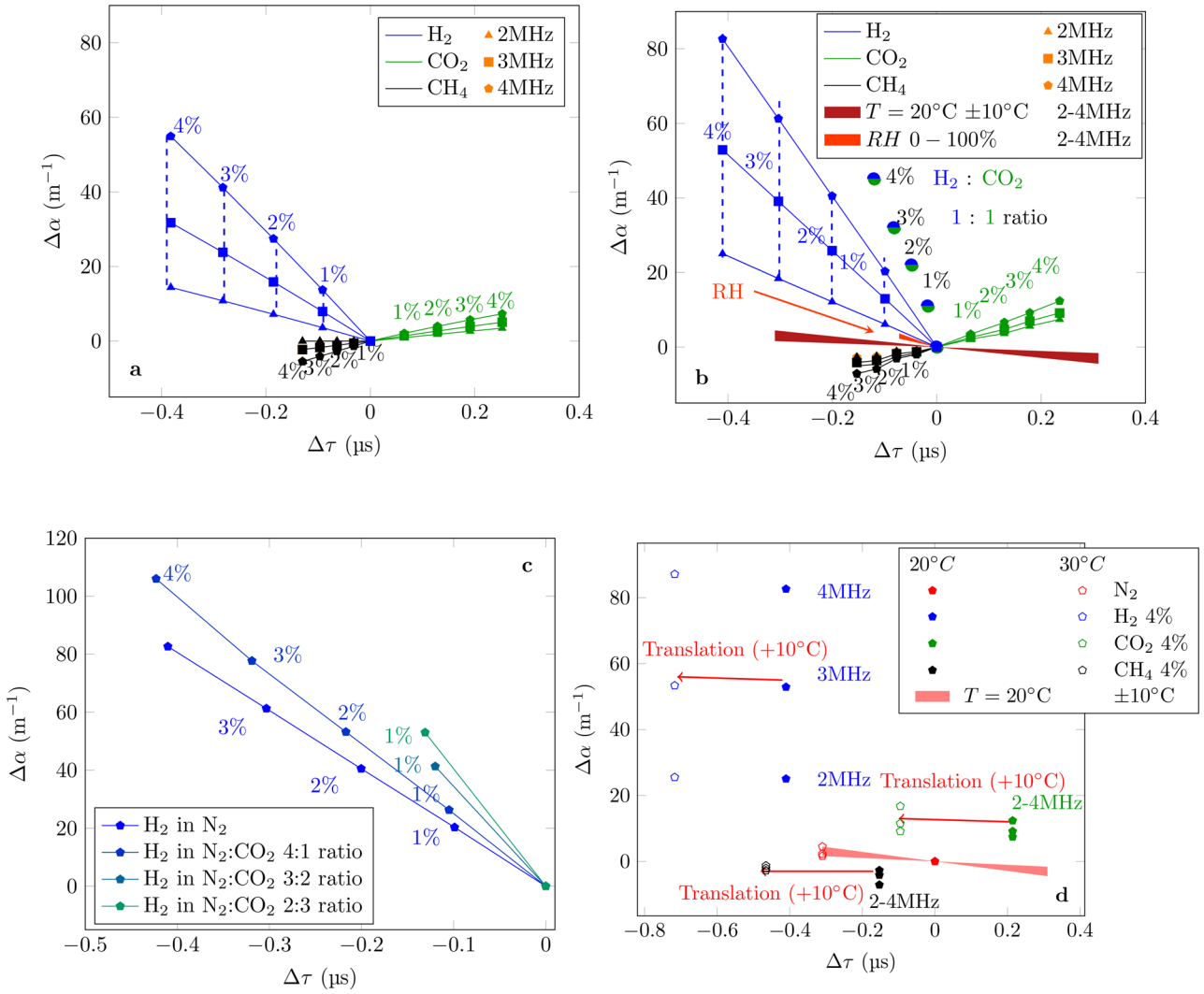

Figure 3. $\Delta\alpha$ as a function of $\Delta\tau$ for different binary gas mixtures. (**a**) Theoretical values. (**b**) Measurements with N_2 as reference gas and either pure contaminant (H_2, CO_2 or CH_4) or mixed contaminant (H_2 with CO_2) at different concentrations. (**c**) Measurements of H_2 at different concentrations under different reference gases mixtures of N_2/CO_2. (**d**) Influence of the temperature on the discrimination resulting in a translation effect.

there seems to be some additional losses than the ones predicted by the linear model from Eq. (14). This is due to the beginning of the relaxation attenuation peak of H_2, which is already an important and non-linear component of the attenuation[8]. Nevertheless, in a practical application, this can be solved with a calibration mapping $\Delta\alpha$ to the molar fraction of H_2 (Fig. 2d).

Discrimination. So far, the measurements of $\Delta\tau$ and $\Delta\alpha$ have been displayed separately. However they are always measured simultaneously. Therefore, one can exploit this in order to identify the different mixtures. Indeed, as it is shown in Fig. 3a, in theory (Eqs. 10 and 14), when plot $\Delta\alpha$ against $\Delta\tau$, the three different types of mixtures are placed in different parts of the plane. Additionally, since in absolute value, S_α increases with the frequency, it is easier to distinguish between them at higher frequencies (4 MHz rather than at 2 MHz). Figure 3b shows the corresponding measurements resulted from the previous characterization as well as the influence of the temperature and humidity, taking into account the cross-sensitivities measured in "Temperature and humidity characterization" section. In the case of the humidity the values above 50% RH were extrapolated to estimate the influence up to 100% RH assuming that the cross-sensitivities of both τ and $\Delta\alpha$ remain constant. Overall the humidity influence remains weak compared to the one of the temperature. In order to illustrate what would happen with a contaminant which is not a pure gas but a mixture of two gases with a fixed constitution (1:1 ratio in this case), measurements of a mixture of H_2 and CO_2 at 4 MHz at different concentrations (1% of the mixture contains 0.5% of each gas) are shown (Fig. 3b). As one would expect, the points fall in between the curves at 4 MHz of each of the constituents. In Fig. 3c, preliminary results at 4 MHz of how the measurements using N_2 as reference gas are modified by using a different reference such as a mixture of N_2 and CO_2 are shown. In fact, if the reference gas is changed, the sensitivities are modified and consequently the slopes of the curves in the plane $(\Delta\alpha, \Delta\tau)$ change as well. However, if the reference gas is known, this can be taken into account during the cali-

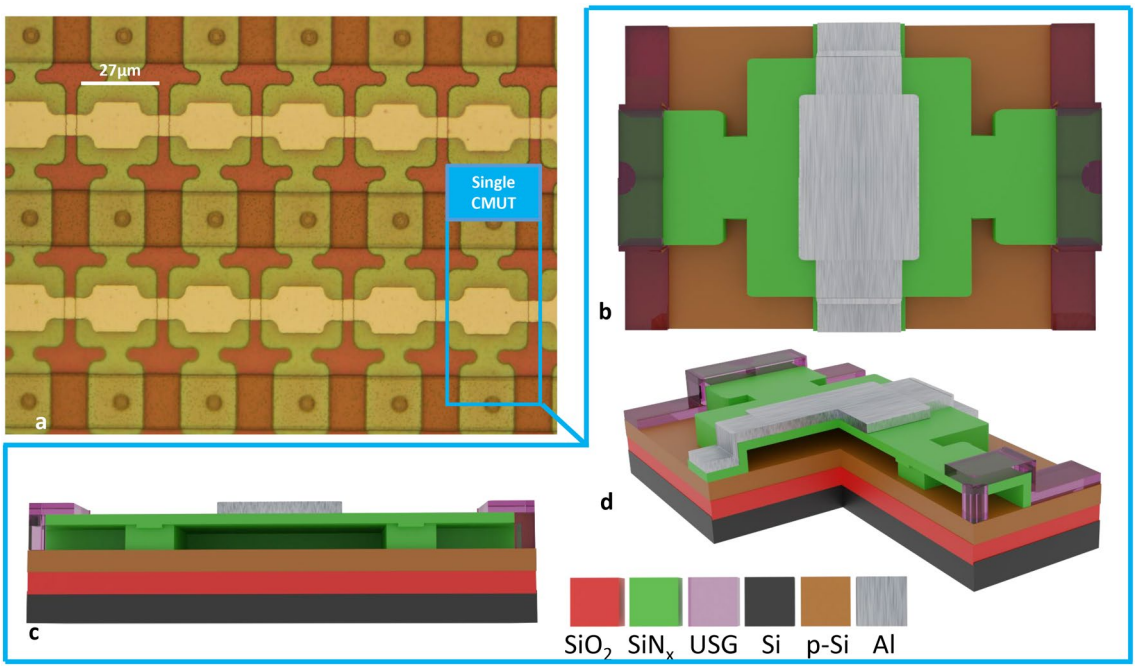

Figure 4. Sensor used in this study. (**a**) Optical microscope image showing part of the CMUT array. (**b**)–(**d**) 3D sketch showing the top view, a transversal cut and a partial cut respectively, where USG stands for Undoped Silicon Glass. Sketch not to scale for visualization purposes.

bration step (Fig. 2c, d). Finally, additional measurements detecting 4% of each of the three mixtures (N_2 with either H_2, CO_2 or CH_4) at 30 °C and at 1, 2 and 3 MHz were performed and displayed with the corresponding measurements at 20 °C in Fig. 3d. From them it can be observed that the main influence of the temperature is an horizontal displacement (shift in τ) with a relatively small displacement along the axis of $\Delta\alpha$.

Discussion

The CMUT ultrasonic gas sensor presented in this paper allows to measure simultaneously both the time of flight and the attenuation coefficient in a binary gas mixture. This allows to discriminate, at a fixed temperature and fixed humidity, between the proposed binary mixtures of N_2 with either H_2, CO_2 or CH_4. Remarkably, a change in the sensor output due to the temperature or humidity can be distinguished by a small change in the attenuation coefficient and a large shift in the time of flight especially for the temperature. This means that, to some extent the sensor presents also temperature or humidity sensor capabilities that can help for numerical compensation. This can be exploited even further by the fact that a slight increase in T from 20 to 30 °C or change in relative humidity results mainly in a substantial decrease in τ with a small shift in $\Delta\alpha$. This means that if a slight loss in accuracy (due to the minor distortion in attenuation caused by either the temperature or the humidity) can be afforded, whenever a change in T or RH is detected (delimited by the dark and light red zones in Fig. 3b), the sensor can perform a self recalibration compensating such effect. Additionally, after the mixture is identified, the concentration can be determined with calibration curves. Concretely, the simultaneous measurement of time of flight and attenuation coefficient with CMUTs results in a robust three binary gas mixtures sensor with built in temperature or humidity sensor capabilities and long term stability. Some potential applications are monitoring of refueling stations, vehicles and nuclear waste storage facilities. Preliminary results in the case of more complex mixture have been presented as well which showed that the calibration step has to be adapted to the application.

Methods

CMUT details. An optical microscope picture of the CMUT array used in this study is shown in Fig. 4 along with 3D schematics from different perspectives of single CMUT. The microfabrication protocol used is similar to the one presented in[25]. Their geometrical characteristics along with polarization and excitation details are given in Table 2.

Setup. The setup to measure both the shift in attenuation, $\Delta\alpha$, and the sound velocity, v, for different gases at different concentrations is shown in Fig. 5. The gases from industrial grade bottles (1) are mixed by a system of flowmeters (2) controlled by a computer (3) at the desired concentrations. The mixture passes through an oven (4) where the desired temperature is set and verified by a thermocouple (5). The gas enters the measurement cell (6) where a continuous ultrasonic sine wave is sent from an emitter CMUT array to a receiver CMUT array after travelling a distance d. Thus, the wave arrives attenuated exponentially with d. Additionally its phase is shifted with respect to the emission by an amount proportional to the time of flight, $\tau = d/v$, required to go through the measuring cell. The receiver is connected to a charge amplifier (7) in order to improve the signal to noise ratio

Membrane size (µm × µm)	27 × 27
Gap (nm)	250
Collapse voltage (V)	98
Reception DC voltage (V)	70
Emission DC voltage (V)	50
Emission AC voltage peak to peak (V)	40
Resonant frequency (MHz)	9.6
Quality factor (×1)	30

Table 2. CMUTs characteristics.

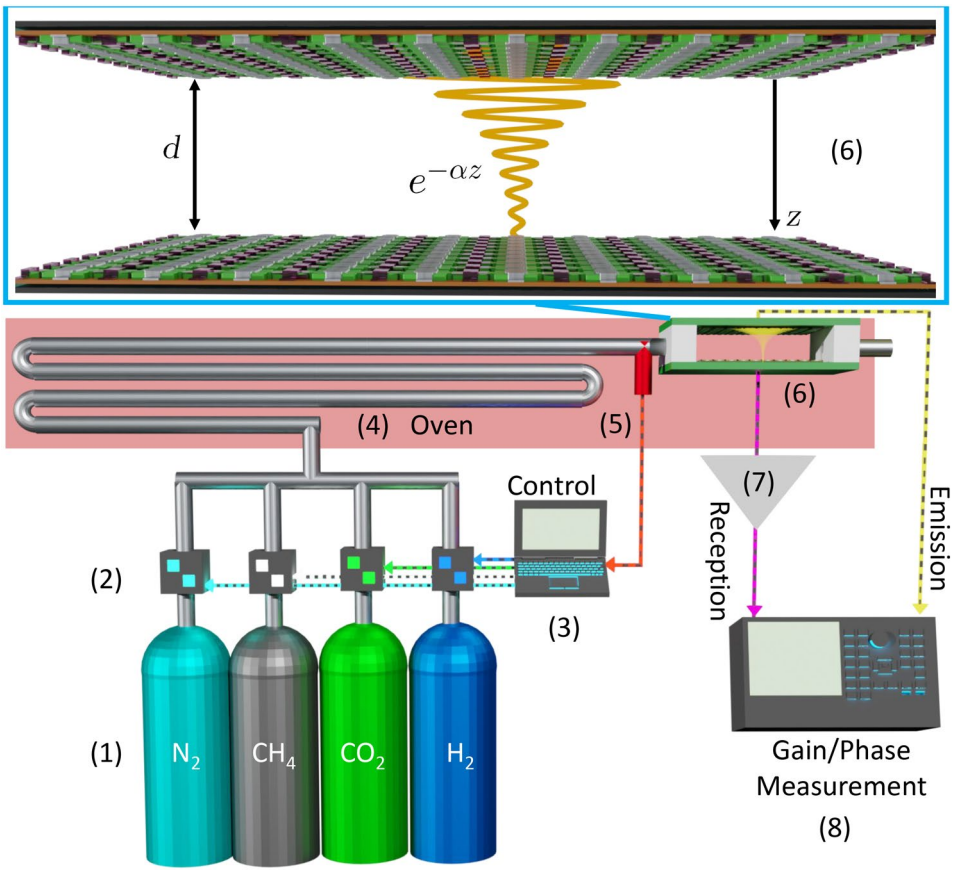

Figure 5. Complete setup schematics. (1) Gas bottles, (2) flowmeters, (3) flow and temperature control computer, (4) oven, (5) thermocouple, (6) measurement cell with zoom at the top of the image, (7) charge amplifier, (8) gain/phase network analyzer.

before being fed along with the emission signal to a gain/phase network analyzer (8). Finally, for the humidity measurements, a vapor generator PUL110 was used to humidify N_2. It should be noted that although the measuring setup presented is rather bulky, more compact components such as the network analyzer can be built[34].

No reflections model. Far from the resonance of the CMUTs, on the side of lower frequencies, one can assume that their electromechanical transfer function is a constant. Thus, using the complex formalism, the pressure wave p can be considered of the form:

$$p(t,z) = P_{00}e^{-\alpha z}e^{j(\omega t - kz)}, \tag{15}$$

where P_{00} is the amplitude of the wave at $t = 0$ on the emission end, ω the excitation angular frequency, $j = \sqrt{-1}$, t the time, z the coordinate orthogonal to the CMUT array (Fig. 5), α the attenuation coefficient of the gas and k the wave number which, in the case of a plane wave, is linked to the gas sound velocity v as follows:

$$k = \frac{\omega}{v}. \tag{16}$$

Since the wave is continuous, at any given time $t_0 \geq \tau$, the value of p at the receiving end ($z = d$) is:

$$p(t_0, d) = P_{00} e^{-\alpha d} e^{j\omega t_0} e^{-j\omega d/v}. \tag{17}$$

Thus, its phase is shifted by a value of $-\omega\tau$ ($\tau = d/v$) with respect to the value of p at the emission end at the same time t_0:

$$p(t_0, 0) = P_{00} e^{j\omega t_0}. \tag{18}$$

The transfer function due only to the setup, H_0, independent of the gas can be defined as:

$$H_0 = |H_0| e^{j\phi_0}, \tag{19}$$

where ϕ_0 is a constant and accounts for the shifts due to the setup and $|H_0|$ is the modulus of H_0, which depends only on the angular frequency. Therefore the total phase shift ϕ is:

$$\phi = -\omega\tau + \phi_0, \tag{20}$$

As a consequence τ is simply the slope of the curve $\phi(\omega)$. Additionally, the change in amplitude is simply $e^{-\alpha d}$. Hence the total gain $|H|$ is given by:

$$|H| = |H_0(j\omega)| e^{-\alpha d}, \tag{21}$$

In order to overcome the need of knowing $|H_0|$, a calibration step was performed to measure $|H|$ under N_2, $|H|_{N2}$. Indeed, the shift in attenuation with respect to N_2, $\Delta\alpha$, is given by:

$$\Delta\alpha = \frac{1}{d} ln \frac{|H|_{N2}}{|H|}, \tag{22}$$

Dealing with multiple reflections. In order to measure a high signal to noise ratio, especially for higher frequencies, it is possible to increase the excitation amplitude. However, this will cause reflections that will interfere with the main emission, particularly for lower frequencies, where the attenuation is smaller. Therefore, they will modify both ϕ and $|H|$. This section seeks to understand the extent of this effect and, particularly, how to retrieve information about both α and τ. Assuming normal incidence and a reflection coefficient of r identical for both CMUT arrays, at a given position z and time t, the acoustic wave in the cell is the superposition of a wave travelling forward p_f (towards increasing z) and one travelling backwards p_b (towards decreasing z). The former is the sum of all the reflections that happen an even number of times (0 included) between the emission time and the measurement time i.e.:

$$p_{f,n} = P_{00} e^{j\omega t} \sum_{i=0}^{n} r^{2i} e^{-(jk+\alpha)(2id+z)}, \tag{23}$$

where n is the echo order (initial 0). Similarly, p_b is the sum of the waves that have been reflected an odd number of times.

$$p_{b,n} = P_{00} e^{j\omega t} \sum_{i=1}^{n} r^{2i-1} e^{-(jk+\alpha)(2id-z)}. \tag{24}$$

Notice that the term of order 0 is not to be accounted since the emission happens only towards the increasing z. Both p_f and p_b are geometric sums of same quotient q given by:

$$q = r^2 e^{-2d(jk+\alpha)}. \tag{25}$$

Since $|q| < 1$, p_f and p_b are simply given by:

$$p_{f,n} = p_{f,0} \frac{1 - q^{n+1}}{1 - q}, \tag{26}$$

$$p_{b,n} = u_0 \left(\frac{1 - q^{n+1}}{1 - q} - 1 \right), \tag{27}$$

where

$$p_{f,0} = P_{00} e^{j(\omega t - kz) - \alpha z} \tag{28}$$

$$u_0 = \frac{1}{r} P_{00} e^{j(\omega t + kz) + \alpha z}. \tag{29}$$

The total acoustic signal is finally

$$p_n = p_{f,n} + p_{b,n}. \tag{30}$$

One can verify that, the case $n = 0$ corresponds exactly to the model presented in "No reflections model" section. In permanent regime, one can consider the number of echoes to be infinite, resulting in the final acoustic signal p_∞:

$$p_\infty(z) = \frac{p_{f,0}(z) + q u_0(z)}{1 - q}. \tag{31}$$

The total transfer function H is then given by:

$$H = -H_0 \frac{p_\infty(z = d)}{P_{00}} \tag{32}$$

which equals:

$$H = -H_0 \frac{(r+1) e^{-j\omega\tau - \alpha d}}{(r e^{-j\omega\tau - \alpha d} - 1)(r e^{-j\omega\tau - \alpha d} + 1)} \tag{33}$$

It should be noticed once again that without any reflections ($r = 0$) $H(j\omega)$ is equal to the transfer function with a single peak:

$$H_{n=0} = H_0 e^{-j\omega\tau - \alpha d}. \tag{34}$$

In order to extract information about α some additional calculations are needed. Indeed, by using the fact that for $|y| < 1$:

$$\frac{1}{1 - y} = \sum_{n=0}^{\infty} y^n, \tag{35}$$

and some basic series manipulations Eq. (33) can be rewritten as:

$$H = \sum_{n=1}^{\infty} P_n e^{-j\omega(2n-1)\tau}, \tag{36}$$

where

$$P_n = H_0 (r+1) r^{2(n-1)} e^{-(2n-1)\alpha d}. \tag{37}$$

It is important to point out that all the P_n are independent of τ. From this form it can be seen that H is the sum of complex exponentials modulated by the functions P_n. Applying the inverse Fourier transform to H (noted $\hat{H}$) defined as:

$$\hat{H} = \int_{-\infty}^{\infty} H(f) e^{2\pi j f t} df, \tag{38}$$

will result in:

$$\hat{H}(t) = \sum_{n=1}^{\infty} \hat{P}_n(t - (2n-1)\tau), \tag{39}$$

where $\hat{P}_n$ is the inverse Fourier transform of P_n. Therefore, $\hat{H}$ is the sum of peaks, where the envelope is the shifted inverse Fourier transform of P_n. In particular, the amplitude of the second peak is given by:

$$P_1 = H_0 (r+1) e^{-\alpha d}. \tag{40}$$

Therefore, by isolating $|P_1|$ it is possible to apply the same formula from the single reflection case (Eq. 22) to retrieve $\Delta\alpha$. Figure 6a shows the measured result of Eq. (38) under pure N_2 as a function of the delay with respect to the emission, t, which is consistent with Eq. (39). It should be noted that, apart from the main peak $\hat{P}_1$ (at $t = \tau$) and the reflected echo $\hat{P}_2$ (at $t = 3\tau$) there is an additional peak at $t = 0$. This is due to an instantaneous electrical coupling between the emitter and the receiver resulting from the high voltages applied[17]. However, since the objective is to isolate P_1, the coupling won't influence the final result. Figure 6b shows the wavelet transform of the measurement from Fig. 6a and shows that the main peak contains more spectral information, since the highest frequencies are no longer present in the reflected echo. This supports the fact that in order to have information about the attenuation at the highest frequencies it is useful, and sometimes necessary, to accept the presence of reflections of the lower frequency components constituting the acoustic wave. However, this perturbs strongly H. This can be appreciated in Fig. 6c,d, which show the comparison between the measured transfer function

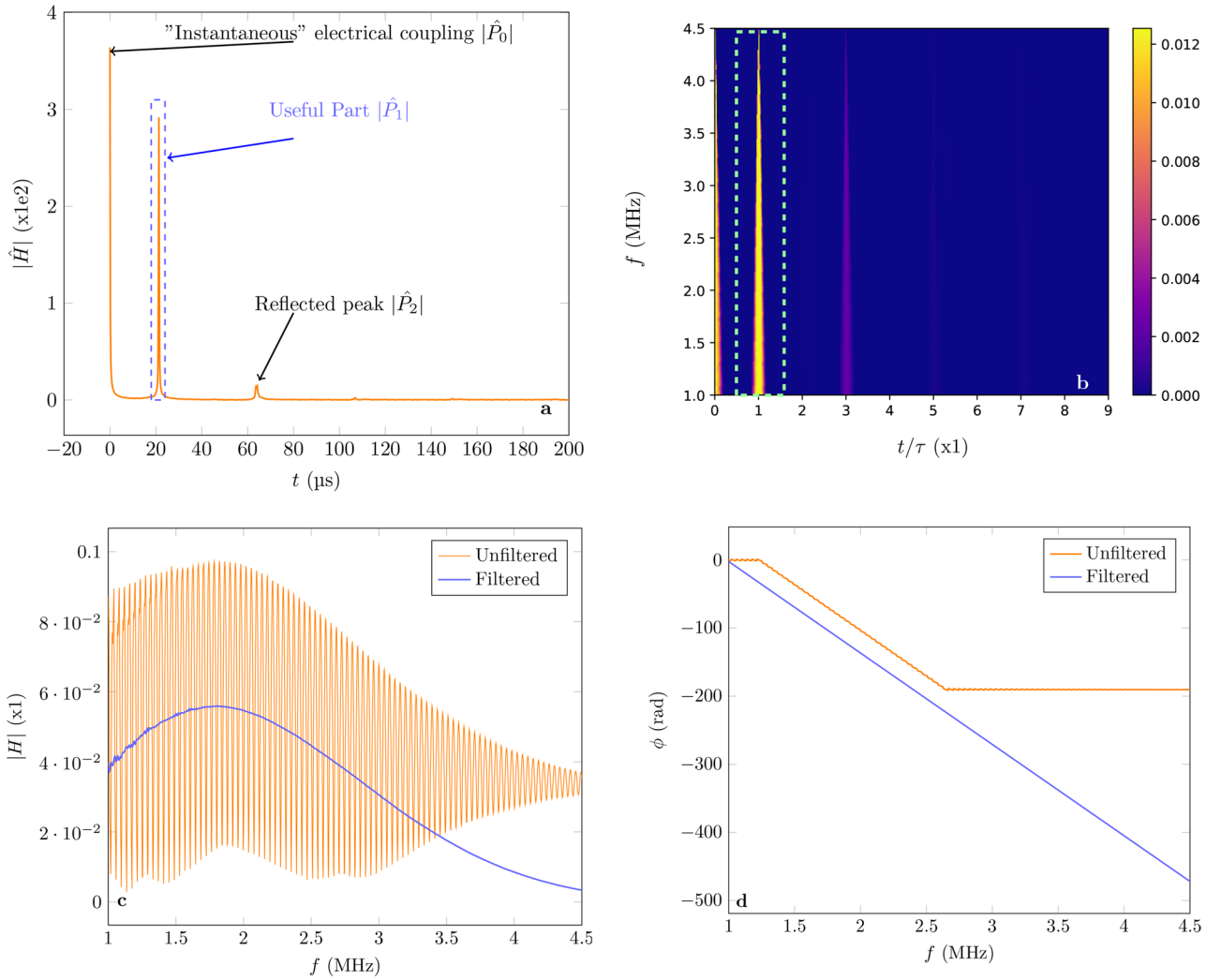

Figure 6. (**a**) Measurement of $|\hat{H}|$ as a function of the delay with respect to the emission. (**b**) Its wavelet transform diagram. (**c**) and (**d**) Comparison between the transfer function for multiple reflections (unfiltered) and after the main echo is extracted (filtered) for the gain and phase, respectively.

(both with multiple reflections and electrical coupling) and the result of the data processing after retrieving only the contribution of P_1 by filtering out components of $\hat{H}$, which are outside of the range $t \in [15, 30]$ µs. This numerical criterion should be modified according to the application (v and d). In our case, τ is not expected to vary more than 1 µs. It should be noted that, after filtering, $|H|$ is smooth as one would expect from the case without reflections. Moreover, the unwrapped (2π-modulo removed) phase after filtering is consistent with the model of a single peak as shown in "Results" section its slope corresponds to $-2\pi\tau$.

Received: 1 September 2021; Accepted: 11 November 2021
Published online: 14 January 2022

References

1. Abdul, S., Judit, T., Ilona, F. & Nikoletta, M. Functional thin films and nanostructures for sensors. In *Fundamentals of Nanoparticles*, 485–519. https://doi.org/10.1016/B978-0-323-51255-8.00016-1 (Elsevier, 2018).
2. Chauhan, P. S. & Bhattacharya, S. Hydrogen gas sensing methods, materials, and approach to achieve parts per billion level detection: A review. *Int. J. Hydrogen Energy* **44**(47), 26076–26099 (2019).
3. Sharma, R. K. *et al.* Investigation of stability and reliability of tin oxide thin-film for integrated micro-machined gas sensor devices. *Sens. Actuators B Chem.* **81**, 9–16 (2001).
4. Hossein-Babaei, F. & Ghafarinia, V. Compensation for the drift-like terms caused by environmental fluctuations in the responses of chemoresistive gas sensors. *Sens. Actuators B Chem.* **143**, 641–648 (2010).
5. Valcárcel, M. *et al.* Optimization of electronic nose drift correction applied to tomato volatile profiling. *Anal. Bioanal. Chem.*https://doi.org/10.1007/s00216-021-03340-5 *(2021).*
6. Sader, J. E. Frequency response of cantilever beams immersed in viscous fluids with applications to the atomic force microscope. *J. Appl. Phys.* **84**, 64–76. https://doi.org/10.1063/1.368002 (1998).
7. Everest, F. A. *The Master Handbook of Acoustics* 4th edn. (McGraw-Hill, 2001).

8. Ejakov, S. G., Phillips, S., Dain, Y., Lueptow, R. M. & Visser, J. H. Acoustic attenuation in gas mixtures with nitrogen: Experimental data and calculations. *J. Acoust. Soc. Am.* **113**, 1871–1879. https://doi.org/10.1121/1.1559177 (2003).
9. Liu, T., Hu, Y., Zhang, X. & Zhu, M. Acoustic analysis of gas compositions based on molecular relaxation features. *Results Phys.* **25**, 104304 (2021).
10. Rosario, R. & Mutharasan, R. Piezoelectric excited millimeter sized cantilever sensors for measuring gas density changes. *Sens. Actuators B Chem.* **192**, 99–104 (2014).
11. Boudjiet, M. *et al.* Geometry optimization of uncoated silicon microcantilever-based gas density sensors. *Sens. Actuators B Chem.* **208**, 600–607 (2015).
12. Suchenek, M. & Borowski, T. Measuring sound speed in gas mixtures using a photoacoustic generator. *Int. J. Thermophys.* **39**, 11. https://doi.org/10.1007/s10765-017-2335-2 (2018).
13. Iglesias, L. *et al.* Proof of concept and preliminary results of gas detection by measuring the admittance at the resonance and anti-resonance of an uncoated CMUT. *Front. Mech. Eng.* **6**, 14. https://doi.org/10.3389/fmech.2020.00014/full (2020).
14. Hök, B., Blückert, A. & Löfving, J. Acoustic gas sensor with ppm resolution. *Sens. Rev.* **20**, 139–142 (2000).
15. Iglesias, L. *et al.* Hydrogen selective gas sensor based on attenuation measurement of acoustic wave using uncoated CMUT. In *2021 IEEE 34th International Conference on Micro Electro Mechanical Systems (MEMS)*, 398–401 (IEEE, 2021). http://ieeexplore.ieee.org/document/9375432/.
16. Iglesias, L., Boudjiet, M. & Dufour, I. Discrimination and concentration measurement of different binary gas mixtures with a simple resonator through viscosity and mass density measurements. *Sens. Actuators B Chem.* **285**, 487–494 (2019).
17. Shanmugam, P. *et al.* Broad bandwidth air-coupled micromachined ultrasonic transducers for gas sensing. *Ultrasonics* **114**, 106410 (2021).
18. Iglesias, L. *et al.* CMUT time of flight gas sensor by phase shift measurement. *IMCS* **MA2020–01**, 2323–2323. https://doi.org/10.1149/MA2020-01312323mtgabs (2020).
19. Törndahl, M., Almqvist, M., Wallman, L., Persson, H. & Lindstrom, K. Characterisation and comparison of a cMUT versus a piezoelectric transducer for air applications. In *2002 IEEE Ultrasonics Symposium, 2002. Proceedings.*, Vol. 2, 1023–1026 (IEEE, 2002). http://ieeexplore.ieee.org/document/1192469/.
20. Engineering ToolBox | http://www.engineeringtoolbox.com/ (2020).
21. Roundy, S., Wright, P. K. & Rabaey, J. A study of low level vibrations as a power source for wireless sensor nodes. *Comput. Commun.* **26**, 1131–1144 (2003).
22. Graves, R. E. & Argrow, B. M. Bulk viscosity: Past to present. *J. Thermophys. Heat Transfer* **13**, 337–342. https://doi.org/10.2514/2.6443 (1999).
23. Zhang, K. *et al.* Calculating vibrational mode contributions to sound absorption in excitable gas mixtures by decomposing multi-relaxation absorption spectroscopy. *Appl. Acoust.* **116**, 195–204 (2017).
24. Law, A. K., Koronaios, N. & Lindsay, R. B. Effect of diffusion on ultrasonic attenuation in mixtures of the rare gases. *J. Acoust. Soc. Am.* **41**, 93–99. https://doi.org/10.1121/1.1910336 (1967).
25. Heller, J., Boulme, A., Alquier, D., Ngo, S. & Certon, D. Performance evaluation of CMUT-based ultrasonic transformers for galvanic isolation. *IEEE Trans. Ultrason. Ferroelectr. Freq. Control* **65**, 617–629 (2018).
26. Cramer, M. S. Numerical estimates for the bulk viscosity of ideal gases. *Phys. Fluids* **24**, 066102. https://doi.org/10.1063/1.4729611 (2012).
27. Wang, Y., Ubachs, W. & van de Water, W. Bulk viscosity of CO_2 from Rayleigh-Brillouin light scattering spectroscopy at 532 nm. *J. Chem. Phys.* **150**, 154502. https://doi.org/10.1063/1.5093541 (2019).
28. Zuckerwar, A. J. & Griffin, W. A. Effect of water vapor on sound absorption in nitrogen at low frequency/pressure ratios. *J. Acoust. Soc. Am.* **69**, 150–154. https://doi.org/10.1121/1.385359 (1981).
29. Winter, T. G. & Hill, G. L. High temperature ultrasonic measurements of rotational relaxation in hydrogen, deuterium, nitrogen, and oxygen. *J. Acoust. Soc. Am.* **42**, 848–858. https://doi.org/10.1121/1.1910657 (1967).
30. Higgins, B. G. & Binous, H. Binary diffusion coefficients for gases. http://demonstrations.wolfram.com/binarydiffusioncoefficientsforgases/ (2020).
31. Bogatyrev, A. F., Belalov, V. R. & Nezovitina, M. A. Thermal diffusion in binary mixtures of moderately dense gases. *J. Eng. Phys. Thermophy* **86**, 1225–1231. https://doi.org/10.1007/s10891-013-0945-5 (2013).
32. Maghari, A. & Hossain Jalili, A. Calculation of transport coefficients for CH_4-N_2 and CH_4-O_2 by the inversion method. *J. Phys. Soc. Jpn.* **73**, 1191–1196. https://doi.org/10.1143/JPSJ.73.1191 (2004).
33. Trengove, R. D., Robjohns, H. L. & Dunlop, P. J. Diffusion coefficients and thermal diffusion factors for the systems H_2–N_2, D_2–N_2, H_2–O_2 and D_2–O_2. *Berichte der Bunsengesellschaft für physikalische Chemie* **87**, 1187–1190. https://doi.org/10.1002/bbpc.19830871220 (1983).
34. Ducrot, P. H., Dufour, I., Nicu, L., Mathieu, F. & Ayela, C. Full system for piezoelectric organic MEMS resonators operating in liquid media. In *Transducers The 19th International Conference on Solid-State Sensors, Actuators and Microsystems*, 1372–1375 (IEEE, 2017). https://doi.org/10.1109/TRANSDUCERS.2017.7994312.

Acknowledgements

This research was performed thanks to the contest Programme d'Investissements d'Avenir of the French Government under the supervision of the French National Radioactive Waste Management Agency (ANDRA).

Author contributions

P.S., J.-F.M., D.A. and D.C. have designed and fabricated the CMUTs. L.I. and I.D. have developed the modeling and data treatments. L.I. has done the measurements. All the authors have contributed to the writing of the paper.

Competing interests

The authors declare no competing interests.

Additional information

Correspondence and requests for materials should be addressed to I.D.

Reprints and permissions information is available at www.nature.com/reprints.

Publisher's note Springer Nature remains neutral with regard to jurisdictional claims in published maps and institutional affiliations.